Role of band states and trap states in the electrical properties of organic semiconductors: Hopping versus mobility edge model

Shafigh Mehraeen, Veaceslav Coropceanu,[*,†] and Jean-Luc Brédas[*,†]
School of Chemistry and Biochemistry and Center for Organic Photonics and Electronics, Georgia Institute of Technology, Atlanta, Georgia 30332-0400, USA
(Received 26 March 2013; published 28 May 2013)

We compare the merits of a hopping model and a mobility edge model in the description of the effect of charge-carrier concentration on the electrical conductivity, carrier mobility, and Fermi energy of organic semiconductors. We consider the case of a composite electronic density of states (DOS) that consists of a superposition of a Gaussian DOS and an exponential DOS. Using kinetic Monte Carlo simulations, we apply the two models in order to interpret the recent experimental data reported for n-doped C_{60} films. While both models are capable of reproducing the experimental data very well and yield qualitatively similar characteristic parameters for the density of states, some discrepancies are found at the quantitative level.

DOI: 10.1103/PhysRevB.87.195209 PACS number(s): 81.05.Fb

I. INTRODUCTION

In spite of recent progress made in controlling the system purity and morphology, most organic electronic thin-film devices still suffer from the presence of significant structural disorder and chemical defects. It was recently shown that a substantial density of localized (trap) states ($\sim 10^{15}$–10^{18} cm^{-3}) is present even in the case of high-mobility organic single crystals such as rubrene and pentacene.[1–5] Therefore, understanding how disorder affects the electrical properties of the system is important in the quest for new materials and devices with improved performance.

In materials with significant disorder, charge transport is usually described in the framework of a hopping model in combination with, for instance, kinetic Monte Carlo (KMC) simulations, the concept of a transport level, effective-medium theory,[6–11] or percolation theory.[12–18] In the hopping regime, charge transport is governed by the thermally activated hopping of charge carriers within the manifold of localized states. An alternative to the hopping model is the mobility edge model.[19,20] In the latter, the electronic states are divided into two nonoverlapping state distributions, one corresponding to localized (trap) states and the other to delocalized (band) states; the two distributions are separated by an energy level referred to as the mobility edge (ME). An additional assumption frequently made within the ME model is that, in contrast to the hopping model, the charge carriers in the localized states are completely immobile; thus, only the carriers that are thermally activated (a multitrap-and-release mechanism) into the band states contribute to charge transport.

An important ingredient of any transport model is the energy spectrum of the electronic system, commonly characterized by the density of states (DOS). In inorganic systems, the DOS of localized band-tail states presents an exponential shape.[21–26] Although an exponential DOS has also been used to interpret the properties of disordered organic semiconductors,[18,27,28] a Gaussian DOS was initially considered and is still more frequently employed for these systems;[12,13,15,29–32] the origin of this choice is that the absorption and fluorescence spectra of disordered organic solids usually display a Gaussian shape.[12,14,33] In addition, hopping models based on a Gaussian DOS predict that, at low carrier concentration, carrier mobility does not depend on charge concentration,[12,34] a feature observed for some polymers.[35]

However, there is now increasing evidence from a number of investigations that, in many organic systems, the deep gap states exhibit an exponential distribution.[1–5,36–38] These studies also suggest that the shallow trap states, i.e. the states located closer to the ME (or the valence band or conduction band edge), deviate from an exponential shape. For instance, very recent results obtained by means of scanning Kelvin probe microscopy on a self-assembled monolayer field-effect transistor (SAMFET) based on quinquethienyl molecules reveal that the DOS consists of an exponential distribution of deep trap states with an additional group of localized shallow states that can be modeled via a Gaussian function.[36] A DOS that can be represented as a superposition of an exponential distribution and a Gaussian distribution has also been recently extracted from the carrier-concentration dependence of the conductivity in C_{60} films.[37] A similar model was used as well to interpret the current-voltage dependence in poly(phenylene vinylene) and in a polyfluorene-based copolymer.[38,39]

The purpose of this paper is to provide a detailed comparison of the hopping model and ME model in describing the effect of charge-carrier concentration on electrical conductivity, carrier mobility, and position of the Fermi level in the case of such a composite DOS. We apply our approach to explain the recent experimental data reported for n-doped C_{60} films.[37]

II. METHODOLOGY

We use a cubic supercell containing $50 \times 50 \times 50$ lattice sites with an intersite distance of 1 nm. The charge-transport properties are simulated using the KMC technique. In our KMC simulations, the electron transfer rate ν_{ij} from site i to site j is described by the Miller–Abrahams model:[40]

$$\nu_{ij} = \nu_0 \exp(-2\gamma r_{ij}) \exp\left(-\frac{\Delta E_{ij} + |\Delta E_{ij}|}{2k_B T}\right). \quad (1)$$

Here, $r_{ij} = |\vec{r}_{ij}|$, $\vec{r}_{ij} = \vec{r}_j - \vec{r}_i$, and $\vec{r}_i$ is the position vector of site i; ν_0 represents the intrinsic attempt frequency; γ the inverse of the localization radius; k_B the Boltzmann

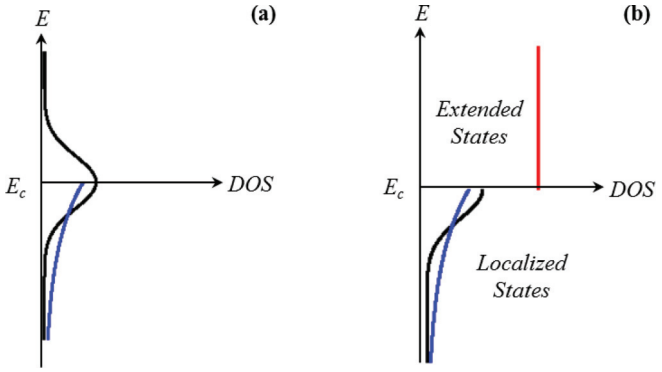

FIG. 1. (Color online) (a) Energetic disorder described by superimposing two distributions, a Gaussian DOS (black) $\rho_G(E)$, centered at E_c, and an exponential DOS (blue) $\rho_E(E)$, positioned below E_c. (b) Description of the DOS in the ME model using a superposition of an exponential (blue) and a half-Gaussian (black) distribution below the ME, and a uniform distribution (red) $\rho_U(E)$, above the ME.

constant; T the temperature; $\Delta E_{ij} = E_j - E_i + e\vec{F}\cdot\vec{r}_{ij}$; and E_i denotes the electron energy at site i. Without loss of generality, the electric field $\vec{F}$ is applied in the negative x direction. Only electron hops between nearest neighbors on the lattice have been taken into account and periodic boundary conditions along all three directions have been applied.

As shown in Fig. 1(a), the energetic spectrum of the system is described by a superposition of: (i) a Gaussian distribution of states, centered around E_c, with a total number of electronic states N_G and a distribution width δ_G:

$$\rho_G(E) = \frac{N_G}{\sqrt{2\pi\delta_G^2}} \exp\left[\frac{-(E-E_c)^2}{2\delta_G^2}\right], \tag{2}$$

and (ii) an exponential distribution of states:

$$\rho_E(E) = \frac{N_E}{\delta_E} \exp\left[\frac{-(E_c-E)}{\delta_E}\right], \quad E \leqslant E_c, \tag{3}$$

where the total number of states and width are given by N_E and δ_E, respectively.

In the KMC simulations, a random Gaussian or exponentially distributed value of energetic disorder taken from Eq. (2) or Eq. (3), respectively, is assigned to each lattice site. Each simulation starts with a random distribution of carriers whose number is given by the electron concentration N_e. Only single electron occupancy on each lattice site is allowed. Since we are mainly interested in charge transport at very low to moderate carrier concentration, we neglect the effect of electrostatic interactions.

We make use of the first reaction method[41,42] in the KMC simulations. At each step of the KMC simulations, we compute the hopping rates for all possible hops of all electrons. The next hop is randomly selected from the derived hopping list. We find the hopping time τ_k for the kth step in the KMC simulation from

$$\tau_k = \frac{-\ln(X)}{\sum_{i,j,i\neq j}^{N} \nu_{ij} L_i}, \tag{4}$$

where N is the total number of sites, L_i is equal to unity if site i is occupied by an electron and zero otherwise, and X is a random number uniformly distributed between 0 and 1 (note that the ν_{ij} values are updated at each time step, and thus indirectly depend on the index k). We run each simulation for a time long enough that the system energy relaxes to a steady-state value, leading to convergence of the electrical conductivity. At this time, we begin to record the time with which we compute conductivity and mobility:

$$\sigma = \frac{e\sum_k x_k}{FL^3\sum_k \tau_k}, \quad \mu = \frac{\sigma}{eN_e} = \frac{\sum_k x_k}{N_e F L^3 \sum_k \tau_k}, \tag{5}$$

where e denotes the unit charge; σ the effective electrical conductivity; μ the effective charge mobility; x_k the x component of the selected hop at time τ_k; and $F = |\vec{F}|$ the magnitude of the applied electric field.

III. RESULTS AND DISCUSSION

It is instructive to consider first the dependence of the electrical conductivity, carrier mobility, and position of the Fermi level on charge density N_e for the case where the energy spectrum can be described solely by either an exponential or a Gaussian DOS. Figure 2 shows the KMC simulation results for conductivity, mobility, and Fermi energy performed at room temperature for several distribution widths ($\delta = 1k_BT$ to $4k_BT$ with intervals of $1k_BT$) assuming $N_G = N_E = 10^{21}$ cm^{-3}. These results, in accordance with the predictions of percolation theory,[18] reveal that, in the case of an exponential DOS and low carrier concentration, the conductivity exhibits a super-linear dependence on charge density,[18] $\sigma \sim (N_e)^{\frac{T_0}{T}}$ (solid black lines) where $T_0 = \delta/k_B$ and $\delta = \delta_E$, as illustrated in Fig. 2(a). Figure 2(a) also indicates that, for the same distribution width and at low carrier concentration, the conductivity using a Gaussian DOS is much larger than that for the exponential DOS. However, in the case of the Gaussian DOS, the conductivity exhibits a less strong dependence on N_e than in the case of the exponential distribution. The significance of the effect that the DOS shape has on charge transport is more clearly seen from the dependence of the effective mobility on charge density [Fig. 2(b)]. The difference is especially evident in the low charge-density limit where the mobility is seen to hardly depend on carrier concentration for a Gaussian DOS while it shows a strong dependence on N_e for an exponential DOS.

We now turn to the dependence of the Fermi level on charge density. The Fermi level E_f is derived from

$$N_e = \int_{-\infty}^{+\infty} \rho(E) f(E, E_f) dE, \tag{6}$$

where $f(E,E_f) = \{1 + \exp[\beta(E-E_f)]\}^{-1}$ represents the Fermi–Dirac distribution and $\beta = (k_BT)^{-1}$. Figure 2(c) shows the impact of DOS on the position of the Fermi level for different distribution widths ranging from $\delta = 1k_BT$ to $4k_BT$. The dependence of the Fermi energy on the charge-carrier concentration is much more pronounced in the case of an exponential DOS than for a Gaussian DOS. The sharper increase in conductivity and Fermi level with charge density in the case of an exponential DOS can be attributed to a

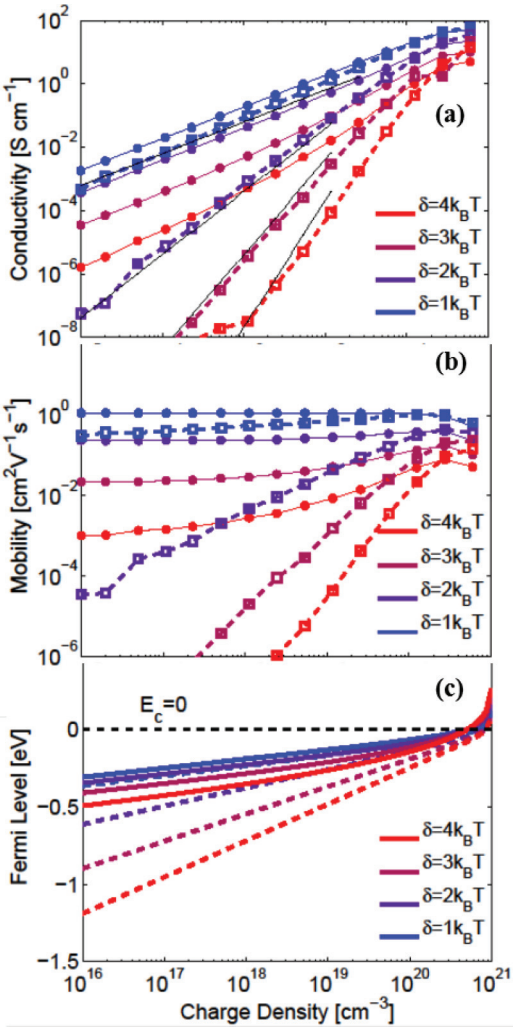

FIG. 2. (Color online) KMC simulation results for (a) conductivity and (b) mobility of charge carriers and (c) analytical results for Fermi level position versus charge density N_e for materials with a Gaussian (solid lines, $\delta = \delta_G$) or an exponential (dashed lines, $\delta = \delta_E$) DOS. Different distribution widths δ are considered, from $1k_BT$ to $4k_BT$, corresponding to blue to red, with $N_G = N_E = 10^{21}$ cm^{-3}. Solid black lines in panel (a) illustrate analytical results for the conductivity $\sigma \sim (N_e)^{\frac{T_0}{T}}$.[18]

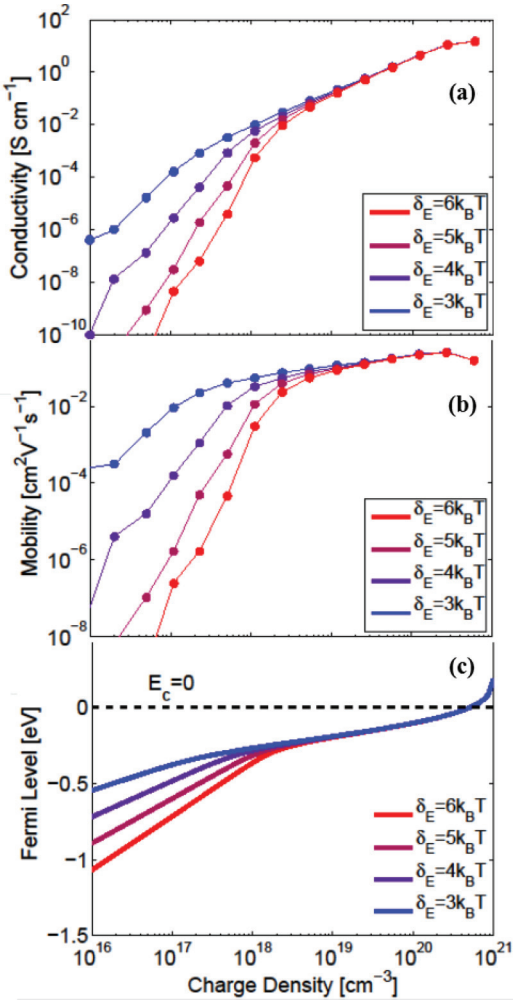

FIG. 3. (Color online) KMC simulation results for (a) conductivity and (b) mobility and (c) analytical results for Fermi level position versus charge density N_e for a superposition of Gaussian and exponential DOS, assuming $N_G = 9.9 \times 10^{20}$ cm^{-3}, $\delta_G = 2.5k_BT$, $N_E = 10^{19}$ cm^{-3} for different δ_E ranging from $3k_BT$ to $6k_BT$, from blue to red.

faster filling of the low-energy states. We note that, in the low charge-carrier concentration limit, the position of the Fermi level can be derived analytically and is given by

$$E_f = \delta_E \left\{ \ln\left[\frac{N_e}{N_E}\right] - \ln\left[\Gamma\left(1-\frac{T}{T_0}\right)\Gamma\left(1+\frac{T}{T_0}\right)\right]\right\}, \quad (7)$$

for an exponential DOS[18,43,44] and by

$$E_f = -\frac{1}{2}\left(\frac{\delta_G^2}{k_BT}\right) + k_BT \ln\left(\frac{N_e}{N_G}\right), \quad (8)$$

for a Gaussian DOS.[45] Here, $\delta_E = k_BT_0$ and Γ is the gamma function. As is apparent from Eqs. (7) and (8) and illustrated in Fig. 2(c), the evolution (slope) of the position of the Fermi level as a function of the logarithm of charge density is determined by the width of the distribution in an exponential DOS and by temperature in a Gaussian DOS.

With the knowledge gained from each individual DOS distribution, we now consider a more complex DOS consisting of a superposition of a Gaussian and an exponential DOS, as shown in Fig. 1(a). The results using a set of parameters similar to that derived for C_{60} films[37] $N_G = 9.9 \times 10^{20}$ cm^{-3}, $\delta_G = 2.5k_BT$, $E_c = 0$, $N_E = 10^{19}$ cm^{-3} and δ_G ranging from $3k_BT$ to $6k_BT$ are illustrated in Figs. 3 and 4. As seen from Fig. 3, it is only at low carrier concentration that the width of the exponential DOS significantly affects the transport properties and the position of the Fermi level. In a similar way, the width of the Gaussian DOS, as seen from Fig. 4, affects the charge-transport characteristics and the Fermi energy only at high carrier concentration, while it has limited impact on the charge-transport properties at low carrier concentrations.

The effects of the ratio of the DOS concentrations (N_E/N_G) on conductivity, carrier mobility, and Fermi energy are illustrated in Fig. 5. The KMC simulations were performed as-

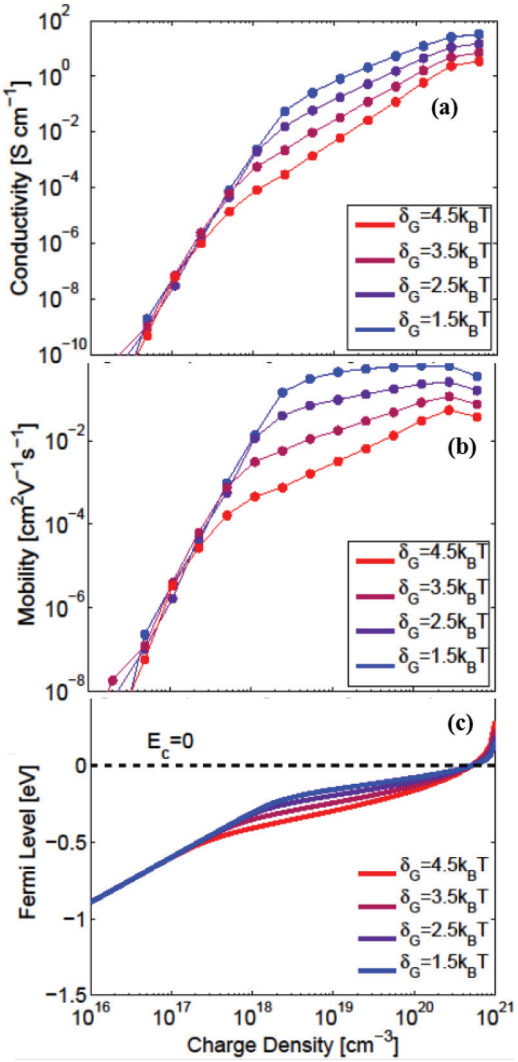

FIG. 4. (Color online) KMC simulation results for (a) conductivity and (b) mobility and (c) analytical results for Fermi level position versus charge density N_e, with fixed $\delta_E = 5k_BT$ for different δ_G ranging from $1.5k_BT$ to $4.5k_BT$, from blue to red (the N_G and N_E values are the same as in Fig. 3: $N_G = 9.9 \times 10^{20}$ cm^{-3}; $N_E = 10^{19}$ cm^{-3}).

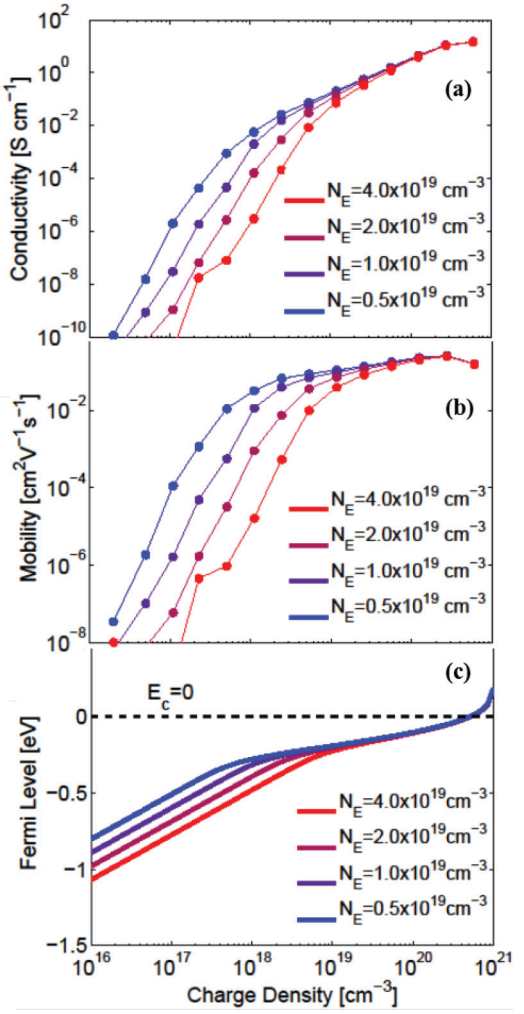

FIG. 5. (Color online) KMC simulation results for (a) conductivity and (b) mobility and (c) analytical results for Fermi level position versus charge density N_e with fixed $\delta_E = 5k_BT$ and $\delta_G = 2.5k_BT$ for different exponential DOS concentrations N_E ranging from 0.5×10^{19} cm^{-3} to 4×10^{19} cm^{-3}, from blue to red, with $N_G + N_E = 10^{21}$ cm^{-3}.

suming $\delta_E = 5k_BT$, $\delta_G = 2.5k_BT$ and different DOS concentrations ($N_E = 0.5 \times 10^{19}$ cm^{-3}, 1.0×10^{19} cm^{-3}, 2.0×10^{19} cm^{-3}, and 4.0×10^{19} cm^{-3}) with the constraint $N_E + N_G = 10^{21}$ cm^{-3}. The results suggest that, while the widths of the DOS define how the evolutions of conductivity, mobility, and Fermi energy depend on charge density in the low and high charge density regimes, the two DOS concentrations define the charge density at which these dependences intersect. As depicted in Fig. 5, changes in the two DOS concentrations do not affect the slopes (parallel line shift). Importantly, the KMC simulation results in Figs. 3–5 illustrate a clear transition in the slopes of the conductivity and carrier mobility as a function of carrier density; a similar transition is also observed for the Fermi level [Fig. 5(c)]. This transition can be explained in the following way. At low carrier concentration, the deep states of the exponential DOS are quickly filled upon initial increase in carrier concentration, leading to a steep rise in the Fermi level and in conductivity. However, at higher carrier concentration, when the Fermi level reaches the point where the Gaussian DOS becomes larger than the exponential DOS, the transport properties and the position of the Fermi level become defined by the Gaussian DOS.

The results described above imply that the charge-transport characteristics at low carrier concentrations are controlled by the distribution of deep traps (exponential distribution), whereas these characteristics at high carrier concentrations are entirely governed by the distribution of states (in the Gaussian distribution) close to the conductive edge (conduction band). Our results also reveal that the electrical conductivity exhibits a transition from super-linear to linear dependence on carrier density at the value of N_e at which the Fermi level reaches the energy where the exponential DOS and Gaussian DOS are approximately equal.

We now turn to the discussion of the ME model. We first consider the case where the states below the ME are solely described by either a half-Gaussian or an exponential

DOS [see Fig. 1(b)]. As mentioned above, according to the ME model,[19,20,46] the total charge density (N_e) is split into mobile (n_M) and immobile (n_I) carriers. In this model, only mobile charges contribute to the overall current and thus to the conductivity. On the basis of the ME model, we obtain the conductivity from

$$\sigma = e n_M \mu_0, \tag{9}$$

where μ_0 is the mobility of mobile charges. In this case, Eq. (6) reads

$$N_e = n_I + n_M = \int_{-\infty}^{0} g(E) f(E, E_f) dE + \int_{0}^{+\infty} \rho_T(E) f(E, E_f) dE, \tag{10}$$

in which $g(E)$ represents the DOS of the states localized below the ME and $\rho_T(E) = N_U$, the DOS of the band states above the ME. Without loss of generality, we assume that the ME is positioned at $E_C = 0$. The conductivity and mobility are then given by

$$\sigma = e\mu_0 \int_{0}^{+\infty} \rho_T(E) f(E, E_f) dE = e\mu_0 N_U k_B T \ln\left[1 + \exp\left(\frac{E_f}{k_B T}\right)\right], \tag{11}$$

and

$$\mu_e = \frac{\sigma}{e N_e} = \frac{\mu_0 N_U k_B T}{N_e} \ln\left[1 + \exp\left(\frac{E_f}{k_B T}\right)\right]. \tag{12}$$

The conductivity, carrier mobility, and Fermi level position are obtained by numerically solving Eqs. (10)–(12). The results are shown in Figs. 6(a)–6(c) and 6(d)–6(f) for Gaussian and exponential DOS, respectively. Along with the numerical results, we also report in Fig. 6 the analytical results obtained in the limit of low carrier concentration (see Appendix). Interestingly, the trends obtained for conductivity, mobility, and Fermi energy are very similar to those obtained using the hopping model (Fig. 2), despite the fact that the localized states

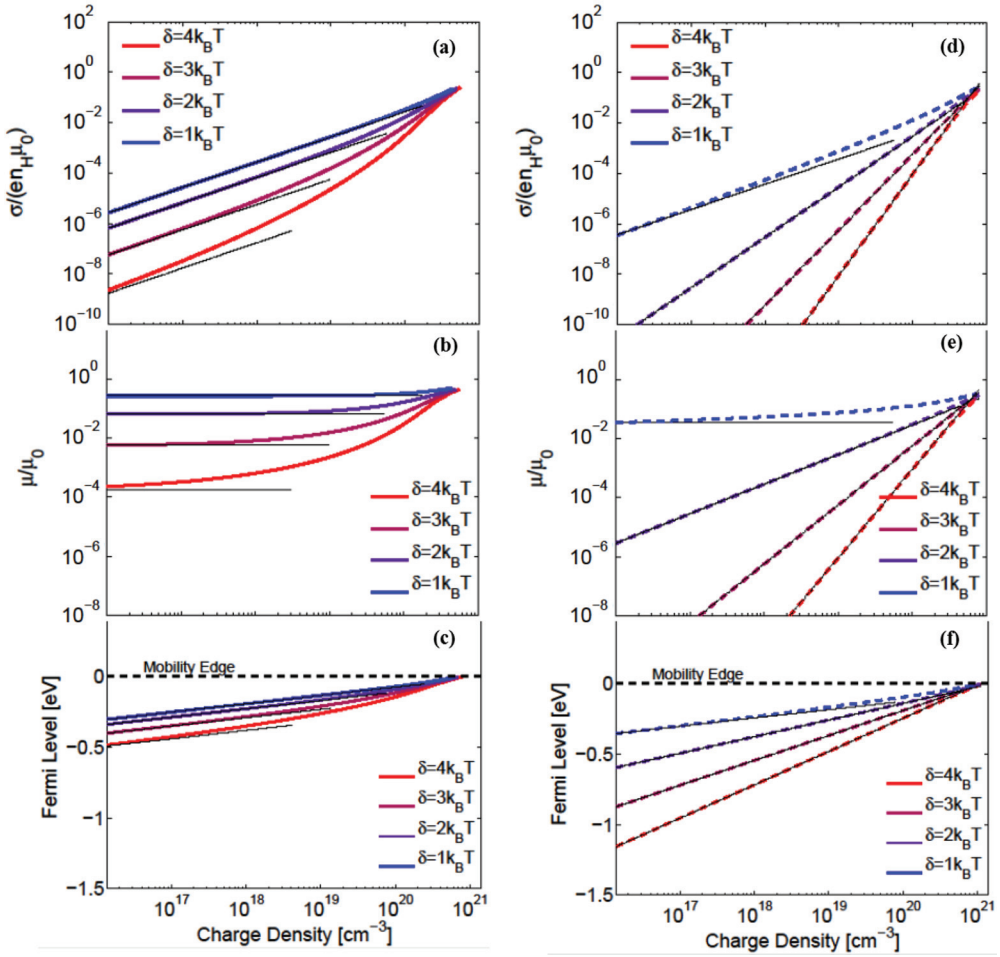

FIG. 6. (Color online) Analytical results of (a) and (d) conductivity, (b) and (e) carrier mobility, and (c) and (f) Fermi level position versus charge density N_e obtained from the ME model using a Gaussian distribution [colored solid lines in (a)–(c)] or an exponential distribution [colored dashed lines in (d)–(f)] of band-tail states below the ME. Different distribution widths $\delta = \delta_G = \delta_E$ are considered and vary from $1k_BT$ to $4k_BT$, from blue to red, respectively, with $N_E = N_G = 10^{21}$ cm^{-3} and $N_U = 2 \times 10^{22}$ cm^{-3} eV^{-1}. The range of agreement between the analytical results and the asymptotic limits at low charge concentration (solid black lines), obtained in Appendix and shown in panels (a)–(c), decreases with δ for a Gaussian DOS.

in the ME model are not directly contributing to transport. This similarity can be rationalized in the following way. In the hopping model, although all states are formally involved in the transport process, charge transport, irrespective of the shape of the DOS distribution, effectively takes place via a so-called transport level[13,16,17] onto which the carriers should be thermally excited. The activation energy rapidly decreases as the carrier concentration increases. In the ME model, however, only charge carriers thermally excited above the ME contribute to the conductivity. Again, the activation energy is a function of the charge density and rapidly decreases as the carrier concentration increases. This means that the transport level in the hopping model is simply replaced by the band states in the ME model. Overall, both models at low and moderate charge carrier concentrations lead to the same trends in the electrical transport properties and position of the Fermi level as a function of charge density.

It is also useful to note that Eqs. (10)–(12) in the limit of low charge density can be solved analytically; the description is given in Appendix. In similarity to the hopping model, the conductivity at low carrier concentration in the ME model exhibits a super-linear dependence on charge density [$\sigma \sim (N_e)^{\frac{T_0}{T}}$] for an exponential DOS [Eq. (A2)] and a linear dependence ($\sigma \sim N_e$) for a Gaussian DOS [Eq. (A8)]. It is also important to note that the ME model predicts, as for the hopping model, that the range of carrier concentration over which the dependence is linear decreases with the increase in δ_G [see Fig. 6(a)].

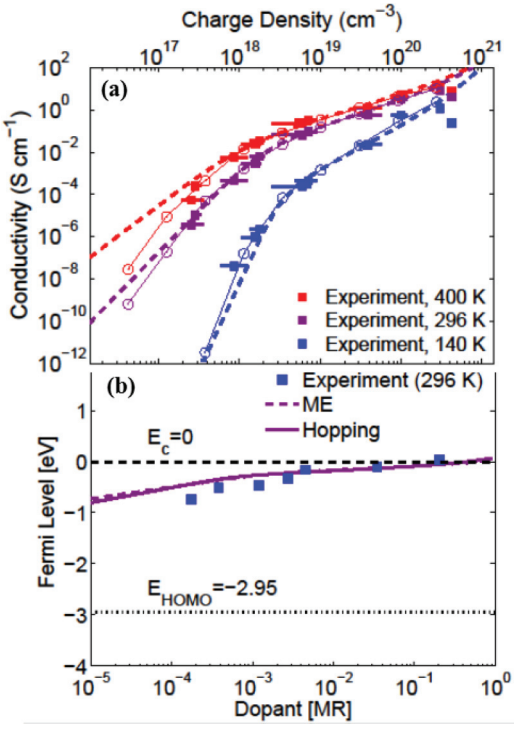

FIG. 7. (Color online) Comparison of (a) conductivity and (b) Fermi level position obtained from experiment (filled squares), the ME model (dashed lines), and the hopping model (solid lines) versus the dopant molar ratio (MR) at three temperatures, 400, 296, and 140 K, corresponding to the red, purple, and blue curves, respectively. In panel (a), error bars for the experimental data are shown by horizontal line segments. In panel (b), the experimental data as well as the HOMO energy (E_{HOMO}) were extracted from UPS measurements.[37]

TABLE I. Parameters obtained from fitting the hopping and ME models to the experimental data[37] reported for n-doped C_{60} films.

Fitting parameters	Hopping model	ME model
N_G (cm^{-3})	0.99×10^{21}	1.6×10^{21}
N_E (cm^{-3})	0.01×10^{21}	0.02×10^{21}
N_U (cm^{-3})		0.8×10^{21}
δ_G/k_BT	2.5	1.8
δ_E/k_BT	5	3.9
T (K)	298	298
F (V cm^{-1})	12,795	
ν_0 (S^{-1})	7×10^{12}	
μ_0 (cm^2 V^{-1} S^{-1})		1.5

In analogy to inorganic semiconductors, the control of charge carrier concentration in organic semiconductors can be achieved by means of molecular doping.[47–52] Here, we apply both hopping and ME models to interpret the recent experimental data reported for n-doped C_{60} films.[37] We note that the carrier concentration in these experiments is derived via a well-controlled n-type doping of the films whereby it can be assumed that each dopant provides one electron to the system; therefore, the electron concentration can be given in terms of the molar ratio (MR) of the dopant versus host. The results obtained from the KMC simulations and from the ME model[19,20,46] are shown in Fig. 7 along with experimental data. For the sake of comparison with the experimental data, axes representing both the dopant MR and the charge density are given in Fig. 7. The parameters derived from the fitting to the experimental data, of the results of the hopping model using KMC simulations and those of the ME model for conductivity are given in Table I. Note that, in the ME model, we construct the band-tail states using a superposition of a half-Gaussian and an exponential distribution. We attribute the overall fitting distribution widths of 2 to $5k_BT$, indicated in Table I, to structural defects and chemical impurities,[1] previously reported for small organic molecules.[3,53,54] A recent study[55] has also shown that the level of such chemical impurities can be reduced, to some extent, by material purification. Figure 7(a) demonstrates that both models are capable of reproducing the dependence of conductivity on charge-carrier concentration over the range of temperatures from 140 to 400 K. Using the parameter set (N_G, N_E, δ_G, and δ_E) obtained above, we also computed the dependence of the Fermi level on charge density $E_f(N_e)$ and compared it to the evolution observed in the ultraviolet photoelectron spectroscopy (UPS) measurements.[37] As seen from Fig. 7(b), a good match between the KMC simulation results of the hopping model, the results of the ME model and the experimental data is again obtained.

IV. CONCLUSIONS

We have compared the performance of a hopping model and a ME model in describing the effect of charge-carrier

concentration on conductivity, mobility, and Fermi level for a composite DOS that consists of a superposition of Gaussian and exponential distributions. Our results indicate that the two models lead to similar trends. In both instances, the charge-transport characteristics at low carrier concentration are controlled by the distribution of deep traps (exponential distribution); at high concentration, these characteristics are entirely governed by the distribution of shallow states (Gaussian distribution). As a result, the charge-transport characteristics show a transition between two different regimes (a super-linear to linear dependence of electrical conductivity on total carrier concentration N_e) at a value of N_e where the Fermi level reaches the energy at which the exponential and Gaussian DOS are approximately equal.

We have applied our approach to interpret the recent experimental data reported on n-doped C_{60} films.[37] Our results indicate that both models can reproduce very well the experimental dependence of electrical conductivity, carrier mobility, and Fermi energy on charge concentration. However, from a quantitative standpoint, some discrepancies arise between the values of the parameters extracted from both models. For instance, the total density of exponential states estimated using the ME model and the hopping model are $N_E = 0.02 \times 10^{21}$ cm^{-3} and 0.01×10^{21} cm^{-3}, respectively. A similar difference is also obtained for $N_G = 0.8 \times 10^{21}$ cm^{-3} (for the sake of comparison, only the states below the reference energy $E_c = 0$ are taken into account) and 0.5×10^{21} cm^{-3} using the ME and hopping model, respectively. These discrepancies arise from the two different pictures of carrier transport, indicating that the suitability of either model for prediction of the charge-transport properties, in particular the electrical conductivity and charge-carrier mobility, requires more experimental data from a wide range of materials.

To summarize, we have shown that, in the range of low and moderate charge carrier concentrations, that is up to carrier concentrations on the order of 10^{17} cm^{-3}, both the hopping and ME models predict similar charge transport characteristics, even in the case of a composite DOS. Therefore, it appears that either model can be utilized to obtain a qualitative description of the distribution of trap states. However, the fact that the ME model can reproduce the experimental data related to electrical transport is not by itself evidence of the existence of band states. In general, a number of other experimental data, for instance, via measurements of the Hall effect, electron spin resonance, or thermoelectric measurements, and those obtained at high charge density are needed in order to gain an in-depth understanding of the nature of the DOS over the whole range of energies.

ACKNOWLEDGMENTS

We thank Antoine Kahn and Selina Olthof for many fruitful discussions. This work has been supported by the King Abdullah University of Science and Technology (KAUST), Award No. KUS-C1-015-21, in the framework of the Center for Advanced Molecular Photovoltaics (CAMP). Computational resources have been provided by the CRIF Program of the National Science Foundation under Award CHE-0946869.

APPENDIX: LOW CHARGE CARRIER CONCENTRATION LIMIT

1. Exponential DOS

Using Eq. (10), we obtain

$$N_e = \frac{N_E}{\delta_E}\int_{-\infty}^{0}\exp\left(\frac{E}{\delta_E}\right)\left[1+\exp\left(\frac{E-E_f}{k_BT}\right)\right]^{-1}dE + N_U k_B T \ln\left[1+\exp\left(\frac{E_f}{k_BT}\right)\right]. \tag{A1}$$

Since at low charge concentration the Fermi level satisfies the condition $-E_f/(k_BT) \gg 1$,[18,43,44] the contribution of the second term in Eq. (A1) (delocalized states) becomes negligible. As a result, E_f is given by Eq. (7), which is similar to that in the hopping model. Using Eqs. (7) and (9), we find the conductivity to correspond to

$$\begin{aligned}\sigma &= e\mu_0 N_U k_B T \ln\left[1+\exp\left(\frac{E_f}{k_BT}\right)\right]\\ &\approx e\mu_0 N_U k_B T \exp\left(\frac{E_f}{k_BT}\right)\\ &\approx e\mu_0 N_U k_B T\left[N_E\Gamma\left(1-\frac{T}{T_0}\right)\Gamma\left(1+\frac{T}{T_0}\right)\right]^{-\frac{T_0}{T}}(N_e)^{\frac{T_0}{T}}.\end{aligned} \tag{A2}$$

Similarly, the mobility is obtained from

$$\begin{aligned}\mu_e &= \frac{\mu_0 N_U k_B T}{N_e}\ln\left[1+\exp\left(\frac{E_f}{k_BT}\right)\right]\\ &\approx \frac{\mu_0 N_U k_B T}{N_e}\exp\left(\frac{E_f}{k_BT}\right)\\ &\approx \mu_0 N_U k_B T\left[N_E\Gamma\left(1-\frac{T}{T_0}\right)\Gamma\left(1+\frac{T}{T_0}\right)\right]^{-\frac{T_0}{T}}(N_e)^{\frac{T_0}{T}-1}.\end{aligned} \tag{A3}$$

Equations (A2) and (A3) are similar to those found within the hopping model using the percolation approach.[18]

2. Gaussian DOS

Replacing the exponential distribution below the ME by a Gaussian distribution in Eq. (A1), we find

$$N_e = \frac{N_G}{\sqrt{2\pi}\delta_G}\int_{-\infty}^{0}\exp\left(-\frac{E^2}{2\delta_G^2}\right)\left[1+\exp\left(\frac{E-E_f}{k_BT}\right)\right]^{-1}dE + N_U k_B T\ln\left[1+\exp\left(\frac{E_f}{k_BT}\right)\right]. \tag{A4}$$

Taking into account that, in the low concentration limit $E_f \ll 0$ and $-E_f/(k_BT) \gg 1$, we obtain

$$N_e \approx C\exp\left(\frac{E_f}{k_BT}\right), \tag{A5}$$

where the constant C is given by

$$C = \left\{ \frac{N_G}{2} \exp\left(\frac{\alpha^2}{2}\right) \left[1 + \mathrm{erf}\left(\frac{\alpha}{\sqrt{2}}\right)\right] + N_U k_B T \right\}. \quad \text{(A6)}$$

Here, erf denotes the error function and $\alpha = \delta_G/(k_B T)$. From Eq. (A5), the Fermi level is given by:

$$E_f \approx k_B T \ln\left(\frac{N_e}{C}\right). \quad \text{(A7)}$$

Using Eqs. (11), (12), and (A7), the conductivity and mobility are written as

$$\sigma \approx e\mu_0 N_U k_B T \exp\left(\frac{E_f}{k_B T}\right) \approx e\mu_0 N_U k_B T \left(\frac{N_e}{C}\right), \quad \text{(A8)}$$

and

$$\mu_e \approx \frac{\mu_0 N_U k_B T}{C}. \quad \text{(A9)}$$

*Corresponding authors: coropceanu@gatech.edu; jean-luc.bredas@chemistry.gatech.edu

†Also affiliated with Department of Chemistry, King Abdulaziz University, Jeddah 21589, Saudi Arabia.

[1] W. L. Kalb, S. Haas, C. Krellner, T. Mathis, and B. Batlogg, Phys. Rev. B **81**, 155315 (2010).
[2] W. L. Kalb, K. Mattenberger, and B. Batlogg, Phys. Rev. B **78**, 035334 (2008).
[3] C. Krellner, S. Haas, C. Goldmann, K. P. Pernstich, D. J. Gundlach, and B. Batlogg, Phys. Rev. B **75**, 245115 (2007).
[4] J. Dacuna, W. Xie, and A. Salleo, Phys. Rev. B **86**, 115202 (2012).
[5] J. Dacuna and A. Salleo, Phys. Rev. B **84**, 195209 (2011).
[6] I. I. Fishchuk, Philos. Mag. B **81**, 561 (2001).
[7] A. Kadashchuk, Y. Skryshevskii, A. Vakhnin, N. Ostapenko, V. I. Arkhipov, E. V. Emelianova, and H. Bassler, Phys. Rev. B **63**, 115205 (2001).
[8] B. Movaghar, M. Grunewald, B. Ries, H. Bassler, and D. Wurtz, Phys. Rev. B **33**, 5545 (1986).
[9] M. Grunewald and P. Thomas, Phys. Status Solidi B **94**, 125 (1979).
[10] I. I. Fishchuk, D. Hertel, H. Bassler, and A. K. Kadashchuk, Phys. Rev. B **65**, 125201 (2002).
[11] M. Grunewald, B. Pohlmann, B. Movaghar, and D. Wurtz, Philos. Mag. B **49**, 341 (1984).
[12] H. Bassler, Phys. Status Solidi B **175**, 15 (1993).
[13] S. Baranovski, *Charge Transport in Disordered Solids with Applications in Electronics* (Wiley, Chichester, England; Hoboken, NJ, 2006).
[14] H. Bassler, Phys. Status Solidi B **107**, 9 (1981).
[15] B. Hartenstein and H. Bassler, J. Non-Cryst. Solids **190**, 112 (1995).
[16] V. I. Arkhipov, E. V. Emelianova, and G. J. Adriaenssens, Phys. Rev. B **64**, 125125 (2001).
[17] V. I. Arkhipov, P. Heremans, E. V. Emelianova, G. J. Adriaenssens, and H. Bassler, J. Non-Cryst. Solids **338**, 603 (2004).
[18] M. C. J. M. Vissenberg and M. Matters, Phys. Rev. B **57**, 12964 (1998).
[19] N. F. Mott, Philos. Mag. **22**, 7 (1970).
[20] N. F. Mott and W. D. Twose, Adv. Phys. **10**, 107 (1961).
[21] D. Monroe, Phys. Rev. Lett. **54**, 146 (1985).
[22] M. Silver and L. Cohen, Phys. Rev. B **15**, 3276 (1977).
[23] F. W. Schmidlin, Solid State Commun. **22**, 451 (1977).
[24] J. Noolandi, Phys. Rev. B **16**, 4466 (1977).
[25] T. Tiedje and A. Rose, Solid State Commun. **37**, 49 (1981).
[26] J. Orenstein, M. A. Kastner, and V. Vaninov, Philos. Mag. B **46**, 23 (1982).
[27] P. M. Borsenberger, L. T. Pautmeier, and H. Bassler, Phys. Rev. B **46**, 12145 (1992).
[28] R. Schwarz, J. Non-Cryst. Solids **227**, 148 (1998).
[29] G. Hadziioannou and P. F. v. Hutten, *Semiconducting Polymers: Chemistry, Physics, and Engineering* (Wiley-VCH, Weinheim, New York, 2000).
[30] M. Pope and C. E. Swenberg, *Electronic Processes in Organic Crystals and Polymers* (Oxford University Press, New York, 1999).
[31] R. Schmechel, Phys. Rev. B **66**, 235206 (2002).
[32] J. Orenstein and M. Kastner, Phys. Rev. Lett. **46**, 1421 (1981).
[33] R. Jankowiak, K. D. Rockwitz, and H. Bassler, J. Phys. Chem. **87**, 552 (1983).
[34] J. O. Oelerich, D. Huemmer, and S. D. Baranovskii, Phys. Rev. Lett. **108**, 226403 (2012).
[35] C. Tanase, P. W. M. Blom, and D. M. de Leeuw, Phys. Rev. B **70**, 193202 (2004).
[36] W. S. C. Roelofs, S. G. J. Mathijssen, R. A. J. Janssen, D. M. de Leeuw, and M. Kemerink, Phys. Rev. B **85**, 085202 (2012).
[37] S. Olthof, S. Mehraeen, S. K. Mohapatra, S. Barlow, V. Coropceanu, J. L. Bredas, S. R. Marder, and A. Kahn, Phys. Rev. Lett. **109**, 176601 (2012).
[38] Y. Zhang, B. de Boer, and P. W. M. Blom, Phys. Rev. B **81**, 085201 (2010).
[39] S. L. M. van Mensfoort, J. Billen, S. I. E. Vulto, R. A. J. Janssen, and R. Coehoorn, Phys. Rev. B **80**, 033202 (2009).
[40] A. Miller and E. Abrahams, Phys. Rev. **120**, 745 (1960).
[41] D. T. Gillespie, J. Phys. Chem. **81**, 2340 (1977).
[42] D. T. Gillespie, J. Comput. Phys. **22**, 403 (1976).
[43] M. Shur and M. Hack, J. Appl. Phys. **55**, 3831 (1984).
[44] O. Marinov, M. J. Deen, and R. Datars, J. Appl. Phys. **106**, 064501 (2009).
[45] S. D. Baranovskii, I. P. Zvyagin, H. Cordes, S. Yamasaki, and P. Thomas, Phys. Status Solidi B **230**, 281 (2002).
[46] A. Salleo, T. W. Chen, A. R. Volkel, Y. Wu, P. Liu, B. S. Ong, and R. A. Street, Phys. Rev. B **70**, 115311 (2004).
[47] R. Schmechel, J. Appl. Phys. **93**, 4653 (2003).
[48] C. K. Chan, W. Zhao, S. Barlow, S. Marder, and A. Kahn, Adv. Polym. Sci. **9**, 575 (2008).
[49] R. C. Haddon, A. F. Hebard, M. J. Rosseinsky, D. W. Murphy, S. J. Duclos, K. B. Lyons, B. Miller, J. M. Rosamilia, R. M. Fleming, A. R. Kortan, S. H. Glarum, A. V. Makhija, A. J. Muller, R. H. Eick, S. M. Zahurak, R. Tycko, G. Dabbagh, and F. A. Thiel, Nature **350**, 320 (1991).

[50]F. H. Li, M. Pfeiffer, A. Werner, K. Harada, K. Leo, N. Hayashi, K. Seki, X. J. Liu, and X. D. Dang, J. Appl. Phys. **100**, 023716 (2006).
[51]T. Menke, D. Ray, J. Meiss, K. Leo, and M. Riede, Appl. Phys. Lett. **100**, 093304 (2012).
[52]M. Pfeiffer, A. Beyer, T. Fritz, and K. Leo, Appl. Phys. Lett. **73**, 3202 (1998).
[53]W. L. Kalb and B. Batlogg, Phys. Rev. B **81**, 035327 (2010).
[54]T. Sueyoshi, H. Fukagawa, M. Ono, S. Kera, and N. Ueno, Appl. Phys. Lett. **95**, 183303 (2009).
[55]S. Olthof, S. Singh, S. K. Mohapatra, S. Barlow, S. R. Marder, B. Kippelen, and A. Kahn, Appl. Phys. Lett. **101**, 253303 (2012).